Analyst

COMMUNICATION

View Article Online
View Journal | View Issue

Cite this: *Analyst*, 2018, **143**, 5352

Received 12th August 2018,
Accepted 19th September 2018

DOI: 10.1039/c8an01555d

rsc.li/analyst

Ultrasensitive electrochemical detection of miRNA based on DNA strand displacement polymerization and Ca^{2+}-dependent DNAzyme cleavage†

Dawei Yang, Wenbo Cheng, Xifeng Chen, Yuguo Tang and Peng Miao *

miRNAs are novel diagnostic and prognostic biomarkers for a diversity of diseases like cancers. In this study, an ultrasensitive electrochemical biosensor for miRNA evaluation is fabricated. A methylene blue (MB) labeled DNA probe is firstly modified on a gold electrode. By employing target induced strand displacement amplification and subsequent DNAzyme cleavage cycles, a large number of MB molecules are released. The decreased oxidation peak current could be used to reveal the miRNA concentration. Based on the two efficient signal amplifications, this method shows ultrahigh sensitivity. Its feasibility for the analysis of miRNA in cell lysates is also demonstrated. Therefore, the method shows attractive potential for promising applications in early diagnosis of certain diseases.

miRNAs are a class of noncoding endogenous ribonucleic acids, which play critical roles in a range of physiological and pathological processes.[1,2] miRNA expression is closely interrelated with gene expression, cell cycle and biological development.[3] Aberrant expression of miRNA is associated with a wide range of diseases, especially cancers. For example, miR-339 promotes the development of stem cell leukemia/lymphoma syndrome (SCLL) through the downregulation of the BCL2L11 and BAX proapoptotic genes;[4] lower expression of miR-613 is found in laryngeal squamous cell carcinoma (LSCC) tissues.[5] miR-141 regulates a range of molecular targets in prostate cancer cells including Rho GTPase family members, which obstructs tumour growth and metastasis.[6] As a consequence, miRNAs have been considered as a new branch of diagnostic and prognostic biomarkers for clinical management.[7] Development of advanced detection methods is of great importance. However, the lengths of miRNAs are about 18 to 25 nucleotides; the abundances of miRNAs in plasma or serum samples are very low with a high degree of sequence similarity. These properties pose difficulties for analytical methods.[8–10]

Conventional techniques for RNA analysis like northern blotting cannot meet the urgent need for miRNA expression analysis due to the low sensitivity and time-consuming procedures. Quantitative reverse transcription polymerase chain reaction (qRT-PCR),[11] microarrays,[12] and RNA sequencing[13] have been developed with much better performances. There are also many other miRNA sensing platforms, which are based on fluorescence,[14] electrochemistry,[15] electrochemiluminescence (ECL),[16] localized surface plasmon resonance (LSPR),[17] and so on. Nevertheless, most of these methods may suffer from shortcomings of low sensitivity, poor specificity and complicated operations. Electrochemical techniques show merits of high sensitivity, low cost, convenient operation and high selectivity, which are highly suitable for miRNA analysis.[18] So far, various electrochemical sensors for miRNA assay have been developed.[19,20] For instance, Fang *et al.* developed a sensitive method for miRNA detection based on a selective binding event between a zinc finger protein and a DNA/RNA hybrid.[21] Zeng *et al.* realized simultaneous detection of multiple miRNAs taking advantage of DNA tetrahedral nanostructures.[22] Crooks's group designed a general electrocatalytic amplification approach for miRNA analysis by single-particle biosensing.[23] However, it is still a challenge to develop ultrasensitive electrochemical biosensors for miRNA analysis.

In this contribution, we have developed an ultrasensitive electrochemical sensing method for amplified detection of miRNA, combining DNA strand displacement polymerization and Ca^{2+}-dependent DNAzyme cleavage cycles. miR-141 is used as the model miRNA. In order to obtain higher sensitivity, signal amplification procedures are necessary,[24] in which nanomaterials or enzymes are usually required.[25,26] DNAzyme is a type of DNA oligonucleotide which is able to realize specific chemical reactions similar to biological enzymes. Metal ions are always required. In this work, a novel type of Ca^{2+}-dependent DNAzyme is involved in enhancing the effect of signal amplification. A detailed sensing principle of

Suzhou Institute of Biomedical Engineering and Technology, Chinese Academy of Sciences, Suzhou 215163, P. R. China. E-mail: miaopeng@sibet.ac.cn

†Electronic supplementary information (ESI) available: Experimental section, Fig. S1–S4 and Table S1. See DOI: 10.1039/c8an01555d

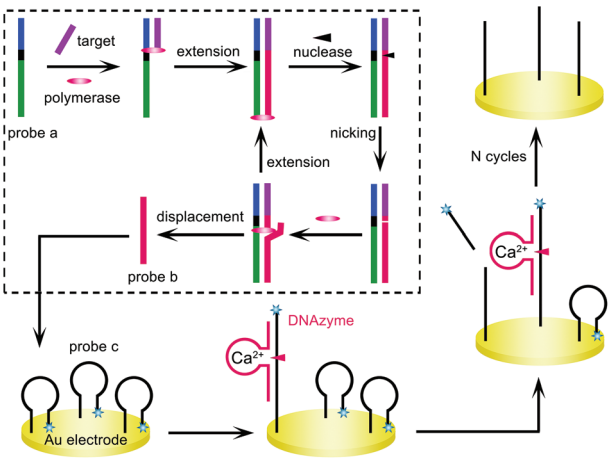

Scheme 1 Illustration of the process of the proposed electrochemical biosensor.

this biosensor is illustrated in Scheme 1. DNA probes are carefully designed for strand displacement polymerization, nicking endonuclease catalyzed cleavage and DNAzyme catalyzed cleavage. Generally, DNA probe a partially hybridizes with target miRNA. The remaining single-stranded region acts as the template for extension, which is catalyzed by a Klenow fragment polymerase. Since the duplex formed contains the restriction site of Nt·BbvCI nicking endonuclease, which is able to cut one strand of the duplex, the polymerization reaction could be continued starting at the strand break. Strand displacement occurs simultaneously, which releases single-stranded DNA probe b. These polymerization–nicking isothermal synergetic reactions are well integrated and can be used to create numerous DNA probe b strands for subsequent reactions. On the other hand, DNA probe c with a hairpin structure is immobilized on a gold electrode *via* Au–S chemistry.[27] *N*-Hydroxysuccinimide ester activated methylene blue (MB) was labeled at the amine-terminated end of DNA probe c, which is used as a redox signal reporter. Due to the hairpin structure, MB gets close to the electrode surface and electron transfer between MB and the electrode is efficient after electrochemical oxidation, which can be reflected in the square wave voltammogram. After the hybridization of DNA probe c and b, DNAzyme is formed. In the presence of Ca^{2+}, a specific cleavage reaction occurs, which releases MB and DNA probe b back to the solution. The free DNA probe b is able to hybridize with the other complete DNA probe c, forming new DNAzyme and cleaving more DNA strands. Due to the remarkable decrease of the amount of MB, the electrochemical signal is significantly declined, which is related to the initial miRNA concentration. Therefore, owing to the dual amplification cycles, an ultrasensitive detection method for miRNA assay is developed.

Chronocoulometry is applied to study the coverage density of the immobilized DNA probe on the electrode surface. According to the Cottrell equation, the chronocoulometric intercept equals the sum of the charge from the reaction of the electrochemical species and the double layer charge.[28] After comparing the chronocoulometry curves (charge *vs.* $t^{1/2}$) of an MCH modified electrode and a DNA probe c modified electrode (Fig. S1†), the DNA density is calculated according to the following equation:

$$\Gamma = Q/nAF$$

in which, Γ represents the density, Q is the calculated charge value, A is the gold area of the electrode, n stands for the number of transferred electrons in a single redox reaction and F is the Faraday constant. The coverage density of DNA probe c is calculated to be 2.17 pmol cm^{-2}.

The reaction pathways of DNA strand displacement amplification and DNAzyme catalyzed amplification are confirmed by polyacrylamide gel electrophoresis (Fig. S2†). The bands of DNA probes a and c are clearly observed (lanes A and E). After the target induced polymerization reaction, the double strand formed appears with a larger molecular weight (lane B). In the presence of nicking endonuclease, a smaller band is observed, which is ascribed to the released DNA probe b by the strand displacement reaction (lane C). On the other hand, after the hybridization event between DNA probes b and c, three bands are observed in the gel image, which are the hybridization product and the two free strands (lane F). However, after the introduction of Ca^{2+}, a cleavage reaction occurs, the band of DNA probe b/c disappears and a new smaller band emerges, which is ascribed to the cleaved product (lane G).

Fabrication of the electrochemical biosensor for the detection of target miRNA is characterized by electrochemical impedance spectroscopy (EIS) and square wave voltammetry (SWV). Fig. 1A shows the Nyquist plots of step by step DNA assembly procedures on the gold electrode. A straight line is observed for the bare electrode, which indicates the excellent conductivity of the gold electrode (curve a). A semicircular portion appears in the spectrum of the DNA probe c modified electrode due to the strong electrostatic repulsion between negatively charged $[Fe(CN)_6]^{3-/4-}$ and the DNA backbone, which confirms the successful DNA immobilization (curve b). Without target miRNA, DNA probe b cannot be produced to hybridize with DNA probe c; thus, no DNAzyme catalyzed reaction occurs and the semicircle diameter of the plot barely changes (curve c). However, after miRNA-triggered reactions, the generated DNA probe b partially hybridizes with DNA probe c. Ca^{2+}-dependent DNAzyme is formed which catalyzes the cleavage reaction and shortens the length of DNA probe c on the electrode, which can be evidenced by the decrease of the semicircle diameter (curve d). SWV is then used to investigate the electrochemistry of methylene blue (MB) during different steps. As shown in Fig. 1B, a flat square wave voltammogram is observed for the bare electrode (curve a). After being modified with DNA probe c, due to the hairpin structure, MB is localized close to the electrode interface; thus a remarkable SWV peak can be obtained (curve b). In the presence of target miRNA, strand displacement amplification occurs and numerous DNA probe b strands are produced for further DNAzyme cleavage. Due to the release of MB, the SWV peak

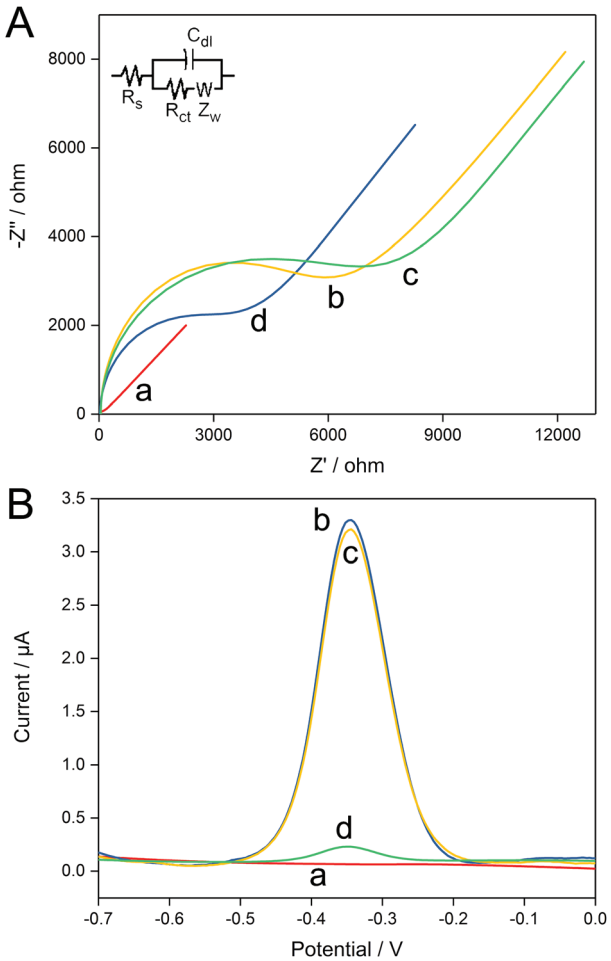

Fig. 1 (A) Nyquist plots and (B) square wave voltammograms corresponding to (a) bare gold electrode and (b) DNA probe c modified electrode, after strand displacement reaction and Ca^{2+}-dependent DNAzyme cleavage (c) without and (d) with target miRNA.

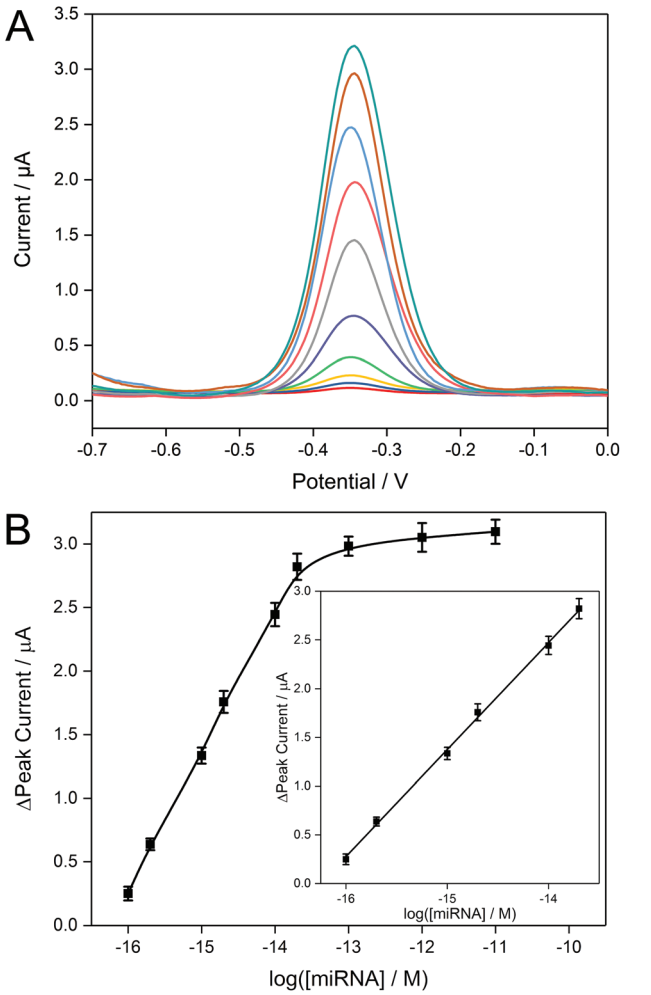

Fig. 2 (A) Square wave voltammograms for the detection of miRNA with the concentrations of 0, 10^{-16}, 2×10^{-15}, 10^{-15}, 2×10^{-14}, 10^{-14}, 2×10^{-13}, 10^{-13}, 10^{-12}, and 10^{-11} M (from top to bottom). (B) Calibration curve that represents the relationship between Δpeak current and miRNA concentration. Inset shows the linear range. Error bars represent the standard deviations of three parallel tests.

decreases significantly (curve d). However, in the absence of miRNA, the peak barely changes (curve c). These results have well demonstrated the feasibility of this biosensor for quantitative analysis of miRNA.

To optimize the used Ca^{2+} and DNAzyme cleavage time, SWV responses are compared (Fig. S3†). 1.2 mM and 60 min are chosen for the following experiments. The sensitivity of this method for electrochemical detection of miRNA is studied by monitoring the SWV responses of MB. As illustrated in Fig. 2A, without target miRNA, no cleavage reaction occurs; thus a SWV curve with a high peak current is achieved. However, with the increasing miRNA concentration from 10^{-16} to 10^{-11} M, the peak current gradually decreases with less MB remaining. The detailed relationship between the decreased peak current and the miRNA concentration is depicted in Fig. 2B. A linear equation is obtained (10^{-16} to 2×10^{-13} M): $y = 17.841 + 1.098\ x$ ($n = 4$, $R^2 = 0.998$), in which y stands for the Δpeak current (μA), x is the logarithmic concentration of the miRNA (M). The limit of detection (LOD) is calculated to be 2.3×10^{-17} M, which is competitive with or even superior to most previously reported miRNA biosensors (Table 1). Since most of the current methods only involve a single amplification process or rely on nanomaterials which may be inhomogeneous, the improvement of sensitivity is limited.[29,30] In contrast, the proposed method integrates two recycle reactions with excellent catalytic efficiencies. A dual amplification strategy is applied. First, target miRNA triggers the polymerization–nicking isothermal synergetic reactions, which may produce a number of DNA probe b strands after strand displacement. Second, DNAzyme composed of DNA probes b and c is able to catalyze DNA cleavage to release the electrochemical species. Meanwhile, DNA probe b is reused for additional cleavage cycles.[31] The combination of the two amplification processes finally enables the analysis of trace miRNA. In addition, since the reaction system contains only commercial enzymes, DNA strands and ions without any inhomogeneous components,

Table 1 Comparison of the analytical performances of recent miRNA assays

Technique	Strategy	Detection range (M)	LOD (M)	Ref.
Colorimetry	Graphene/gold-nanoparticle hybrids	10^{-8} to 9.8×10^{-7}	3.2×10^{-9}	32
Fluorescence	Target-catalyzed hairpin assembly	0 to 1.6×10^{-8}	4.7×10^{-11}	33
Fluorescence	Free-energy-driven lock/open DNA assembly	10^{-12} to 1.5×10^{-8}	2.4×10^{-11}	34
Nanopore	Triplex molecular beacon	0 to 10^{-7}	5×10^{-12}	35
Fluorescence	Polydopamine nanosphere/gold nanocluster based system	10^{-11} to 2.5×10^{-9}	3.6×10^{-12}	36
SPR	High-performance hairpin stacking circuits	2.5×10^{-12} to 2.5×10^{-7}	1.5×10^{-12}	37
Electrochemistry	Self-assembly of redox transducer and DNA anchoring group	10^{-13} to 5×10^{-9}	10^{-13}	38
LSPR	3D plasmonic nanostructure	1.3×10^{-14} to 5×10^{-8}	1.3×10^{-14}	39
Electrophoresis	Separation-assisted double cycling signal amplification	2×10^{-14} to 2×10^{-11}	8×10^{-15}	40
ECL	3D DNA walking machine	10^{-14} to 10^{-10}	3.3×10^{-15}	41
SPR	Au@Ag nanorod etching	5×10^{-17} to 10^{-11}	5×10^{-17}	42
Electrochemistry	Duplex-specific nuclease and catalytic hairpin assembly	10^{-16} to 10^{-8}	2.51×10^{-17}	43
Electrochemistry	Strand displacement reaction and Ca^{2+}-dependent DNAzyme	10^{-16} to 2×10^{-13}	2.3×10^{-17}	This work

excellent reproducibility may be guaranteed. Run-to-run and electrode-to-electrode reproducibility is determined by the detection of three levels of miRNAs with repeated modification of a single electrode and four independent electrodes. The results show excellent consistence (Fig. S4†). This developed sensor is also highly stable. After storing in 10 mM Tris-HCl buffer (10 mM TCEP, 1 mM EDTA, and 0.1 M NaCl) at 4 °C for 1 month, the DNA modified electrode can still be used showing nearly 100% signal intensity.

The selectivity of the proposed method is then investigated by introducing miR-141-1a, miR-141-1b, miR-141-1c, miR-141-2a and miR-141-2b instead of target miR-141. The results of the experiment show that these miRNAs cannot trigger the expected reactions; thus negligible Δpeak currents are measured. Only target miRNA causes a significantly decreased peak current (Fig. 3). It is concluded that the developed method can successfully distinguish target miRNA from possible interfering miRNAs with even single-base-mismatch. Moreover, this method is further challenged with complex biological samples. Human bladder cancer T24 cells were obtained from the Institute of Biochemistry and Cell Biology, Chinese Academy of Sciences, which were lysed and analyzed. Four independent measurements are conducted on three lysate samples. As shown in Table 2, the concentrations are found to be between 0.78 and 1.61 pM. The relative standard deviations are lower than 5%. The recoveries are in the range of 96.3% to 103.21%. We also spiked 5 pM miRNA in the samples, which were then detected with satisfactory results. The proposed method is confirmed to hold great promise for the analysis of miRNA in cancer cells.

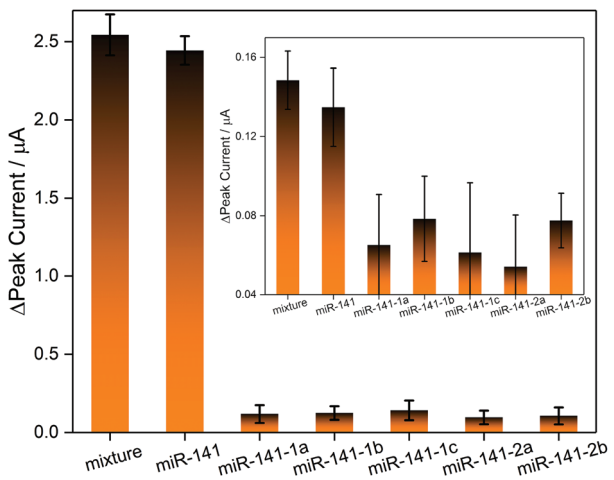

Fig. 3 Specificity of the method for the detection of 10 fM target miRNA. Inset shows the specificity investigation for the detection of 23 aM target miRNA. The concentrations of all interfering miRNAs are 100 times higher.

Conclusions

In summary, a novel electrochemical strategy for miRNA assay with dual amplifications is introduced. In this analytical system, miRNA induced strand displacement polymerization and nicking reactions produce a large number of Ca^{2+}-dependent DNAzyme sequences, which further catalyze the cleavage of MB-labeled DNA. miRNA concentrations from 10^{-16} to 2×10^{-13} M could be readily determined and the LOD is estimated to be 2.3×10^{-17} M. The proof-of-concept experiments verify that the proposed method exhibits excellent sensitivity and selectivity in both ideal buffer and real samples. It is believed

Table 2 Detected results for miRNA quantification in the cell lysates

Sample	Detected (pM)	Relative standard deviation (%)	qRT-PCR (pM)	Recovery (%)	Added (pM)	Detected (pM)	Relative standard deviation (%)
1	0.78	3.12	0.76	102.63	5	5.81	4.77
2	1.04	2.33	1.08	96.30	5	6.09	3.91
3	1.61	4.02	1.56	103.21	5	6.58	3.46

that, this biosensor has great potential for biomedical research and clinical diagnostics after certain modifications.

Conflicts of interest

There are no conflicts to declare.

Acknowledgements

This work is supported by the National Natural Science Foundation of China (Grant No. 81771929 and 81801792), the Scientific Research Instrument Developing Project of the Chinese Academy of Sciences (Grant No. YJKYYQ20170067) and the Natural Science Foundation of Tianjin (Grant No. 17JCQNJC13900).

Notes and references

1 D. P. Bartel, *Cell*, 2004, **116**, 281–297.
2 S. Rachagani, M. A. Macha, N. Heimann, P. Seshacharyulu, D. Haridas, S. Chugh and S. K. Batra, *Adv. Drug Delivery Rev.*, 2015, **81**, 16–33.
3 B. Wang, D. P. Li, I. Kovalchuk, I. J. Apel, A. M. Chinnaiyan, R. K. Woycicki, C. R. Cantor and O. Kovalchuk, *Proc. Natl. Acad. Sci. U. S. A.*, 2018, **115**, 7392–7397.
4 T. X. Hu, Y. T. Chong, S. M. Lu, R. Wang, H. Y. Qin, J. Silva, E. Kitamura, C. S. Chang, L. Hawthorn and J. K. Cowell, *Cancer Res.*, 2018, **78**, 3522–3531.
5 J. Wang, S. J. Yang, W. S. Ge, Y. Wang, C. D. Han and M. C. Li, *J. Cell. Biochem.*, 2018, **119**, 5118–5125.
6 C. Liu, R. F. Liu, D. X. Zhang, Q. Deng, B. G. Liu, H. P. Chao, K. Rycaj, Y. Takata, K. Lin, Y. Lu, Y. Zhong, J. Krolewski, J. J. Shen and D. G. Tang, *Nat. Commun.*, 2017, **8**, 14270.
7 H. Schwarzenbach, D. S. B. Hoon and K. Pantel, *Nat. Rev. Cancer*, 2011, **11**, 426–437.
8 T. Hou, W. Li, X. J. Liu and F. Li, *Anal. Chem.*, 2015, **87**, 11368–11374.
9 P. P. Gai, C. C. Gu, T. Hou and F. Li, *ACS Appl. Mater. Interfaces*, 2018, **10**, 9325–9331.
10 S. Guo, W. N. Lin, Y. W. Hu, G. Y. Sun, D. T. Phan and C. H. Chen, *Lab Chip*, 2018, **18**, 1914–1920.
11 S. Adhikari, M. Turner and S. Subramanian, *Mol. Plant*, 2013, **6**, 229–231.
12 P. T. Nelson, D. A. Baldwin, L. M. Scearce, J. C. Oberholtzer, J. W. Tobias and Z. Mourelatos, *Nat. Methods*, 2004, **1**, 155–161.
13 L. Xie, Z. H. Yao, Y. Zhang, D. Q. Li, F. D. Hu, Y. D. Liao, L. Zhou, Y. H. Zhou, Z. Y. Huang, Z. W. He, L. Han, Y. H. Yang and Z. Z. Yang, *Cell Death Dis.*, 2018, **9**, 772.
14 F. Degliangeli, P. Kshirsagar, V. Brunetti, P. P. Pompa and R. Fiammengo, *J. Am. Chem. Soc.*, 2014, **136**, 2264–2267.
15 H. S. Yin, Y. L. Zhou, C. X. Chen, L. S. Zhu and S. Y. Ai, *Analyst*, 2012, **137**, 1389–1395.
16 M. H. Shamsi, K. Choi, A. H. C. Ng, M. D. Chamberlain and A. R. Wheeler, *Biosens. Bioelectron.*, 2016, **77**, 845–852.
17 P. Miao, Y. G. Tang, Z. Q. Mao and Y. Z. Liu, *Part. Part. Syst. Charact.*, 2017, **34**, 1600405.
18 Z. C. Fang, L. Soleymani, G. Pampalakis, M. Yoshimoto, J. A. Squire, E. H. Sargent and S. O. Kelley, *ACS Nano*, 2009, **3**, 3207–3213.
19 M. N. Islam, M. K. Masud, M. H. Haque, M. S. A. Hossain, Y. Yamauchi, N. T. Nguyen and M. J. A. Shiddiky, *Small Methods*, 2017, **1**, 1700131.
20 S. J. Smith, C. R. Nemr and S. O. Kelley, *J. Am. Chem. Soc.*, 2017, **139**, 1020–1028.
21 C. S. Fang, K. S. Kim, B. Yu, S. Jon, M. S. Kim and H. Yang, *Anal. Chem.*, 2017, **89**, 2024–2031.
22 D. D. Zeng, Z. H. Wang, Z. Q. Meng, P. Wang, L. L. San, W. Wang, A. Aldalbahi, L. Li, J. W. Shen and X. Q. Mi, *ACS Appl. Mater. Interfaces*, 2017, **9**, 24118–24125.
23 A. D. Castaneda, N. J. Brenes, A. Kondajji and R. M. Crooks, *J. Am. Chem. Soc.*, 2017, **139**, 7657–7664.
24 R. M. Graybill, M. C. Cardenosa-Rubio, H. W. Yang, M. D. Johnson and R. C. Bailey, *Anal. Methods*, 2018, **10**, 1618–1623.
25 P. Miao, Y. G. Tang, B. D. Wang, J. Yin and L. M. Ning, *TrAC, Trends Anal. Chem.*, 2015, **67**, 1–15.
26 Y. W. Li, Y. R. Huang, Z. Wang, F. Carniato, Y. J. Xie, J. P. Patterson, M. P. Thompson, C. M. Andolina, T. B. Ditri, J. E. Millstone, J. S. Figueroa, J. D. Rinehart, M. Scadeng, M. Botta and N. C. Gianneschi, *Small*, 2016, **12**, 668–677.
27 Y. J. Yu, Q. Zhang, J. Buscaglia, C. C. Chang, Y. Liu, Z. H. Yang, Y. C. Guo, Y. T. Wang, K. Levon and M. Rafailovich, *Analyst*, 2016, **141**, 4424–4431.
28 P. Miao, Y. T. Jiang, T. Zhang, Y. Huang and Y. G. Tang, *Chem. Commun.*, 2018, **54**, 7366–7369.
29 D. A. Smith, L. J. Newbury, G. Drago, T. Bowen and J. E. Redman, *Sens. Actuators, B*, 2017, **253**, 335–341.
30 Q. Li, Q. Wang, X. H. Yang, K. M. Wang, H. Zhang and W. Y. Nie, *Talanta*, 2017, **174**, 521–526.
31 L. Li, X. Y. Ma, W. F. Dong, P. Miao and Y. G. Tang, *Bioconjugate Chem.*, 2018, **29**, 1021–1024.
32 H. M. Zhao, Y. P. Qu, F. Yuan and X. Quan, *Anal. Methods*, 2016, **8**, 2005–2012.
33 S. J. Zhen, X. Xiao, C. H. Li and C. Z. Huang, *Anal. Chem.*, 2017, **89**, 8766–8771.
34 X. Y. Zhu, R. Y. Wang, X. H. Zhou and H. C. Shi, *ACS Appl. Mater. Interfaces*, 2017, **9**, 25789–25795.
35 X. Y. Wu, B. Y. Guo, Y. Y. Sheng, Y. Zhang, J. Wang, S. C. Peng, L. Liu and H. C. Wu, *Chem. Commun.*, 2018, **54**, 7673–7676.
36 S. H. Xu, Y. Y. Nie, L. P. Jiang, J. Wang, G. Y. Xu, W. Wang and X. L. Luo, *Anal. Chem.*, 2018, **90**, 4039–4045.
37 Y. L. Xing, X. M. Li, T. X. Yuan, W. Cheng, D. D. Li, T. X. Yu, X. J. Ding and S. J. Ding, *Analyst*, 2017, **142**, 4834–4842.

38 H. V. Tran, N. D. Nguyen, B. Piroc and L. T. Tran, *Anal. Methods*, 2017, **9**, 2696–2702.
39 H. K. Na, J. S. Wi, H. Y. Son, J. G. Ok, Y. M. Huh and T. G. Lee, *Biosens. Bioelectron.*, 2018, **113**, 39–45.
40 K. J. Wei, J. J. Zhao, X. S. Luo, S. H. Qiu, F. Y. He, S. T. Li and S. L. Zhao, *Analyst*, 2018, **143**, 1468–1474.
41 Z. Q. Xu, L. L. Liao, Y. Q. Chai, H. J. Wang and R. Yuan, *Anal. Chem.*, 2017, **89**, 8282–8287.
42 Y. Gu, J. Song, M. X. Li, T. T. Zhang, W. Zhao, J. J. Xu, M. L. Liu and H. Y. Chen, *Anal. Chem.*, 2017, **89**, 10585–10591.
43 S. Yu, Y. Y. Wang, L. P. Jiang, S. Bi and J. J. Zhu, *Anal. Chem.*, 2018, **90**, 4544–4551.